RESPONSES OF BED MORPHOLOGY AND CONGESTION PATTERNS WITH DRIFTWOOD ON SAND BARS

TAEUN KANG
Kyoto University, Kyoto, Japan, kangxodns@gmail.com

ICHIRO KIMURA
University of Toyama, Japan. ichiro@sus.u-toyama.ac.jp

SHINICHIRO ONDA
Kyoto University, Kyoto, Japan, onda.shinichiro.2e@kyoto-u.ac.jp

ABSTRACT

The numerical simulations and the flume experiments were conducted for investigation of driftwood deposition patterns and the channel bed deformations. In the study, we generated an alternating bar under the 1.1 liter/s inlet flow discharge and the 0.005 m/m channel slope. The experimental and computational flumes are 12 × 0.4 m^2 and 5 × 0.4 m^2, respectively. The uniform grain size was 0.51 mm. As for the computation, we used the 2D (two-dimensional) depth-averaged flow model, called Nays2DH of the iRIC software to calculate water flows. Nays2DH is a Eulerian model for water flows. For the driftwood dynamics, a Lagrangian type driftwood model as connected spherical shaped particles is coupled with Nays2DH. In the experiments and the simulations, we considered the root wad effect by using a cross shape of root wad and a larger size for a particle at a head of driftwood, respectively. As for the simulations for wood collisions, we used a discrete element method (DEM). Through the study, we obtained the bed profile before/after the driftwood supplies in the laboratory test. The results showed that the speed of bar migration is locally changed by wood jams because the wood jams disturb the water flow. The wood jams can deform alternating bar into mid-channel bar when it is generated at the centre part of the channel. In addition, the smaller time interval of wood supply increases the wood collisions and decreases the number of stored wood pieces. Those results would be informative to study the morphodynamics with driftwood in rivers.

Keywords: Driftwood model, Bed deformation, Congestion pattern, Moveable sand bars, Numerical simulation

1. INTRODUCTION

During recent decades, driftwood (large wood) studies have been actively conducted by three main methodologies such as field observations, flume experiments, and numerical computations. In particular, the driftwood studies were advanced by several countries (e.g., Europe, the US, Japan) to control the driftwood generation together with the disasters. Due to those studies, our knowledge of driftwood has been dramatically enhanced.

At the initial stage of the driftwood study, Braudrick et al. (1997) and Braudrick and Grant (2001) established the basic frame for methodologies about the driftwood dynamics using flume experiments. Braudrick et al. (1997) conducted diverse wood transportations in river and clarified jamming types, such as the uncongested, congested and semi-congested. In addition, Braudrick and Grant (2001) showed the flume experiments to examine parameter interactions among hydraulics, channel formation, travel distance and spatial deposition of wood motions.

Most driftwood studies have discussed that the shape of driftwood is cylindrical in experiments and numerical computations. This shape of driftwood is examined by a hydrodynamic response in an open-channel flow to consider a wood motion for the horizontal orientation along with the submerged volume/area affecting drag force.

The drag force interacting between driftwood and water flow is an important parameter to understand the wood motion. Several researchers (e.g., Gippel et al. 1992; Shields and Alonso, 2010; Persi et al., 2019) have examined the changes of the drag force coefficient depending on the orientation angles along with the cylindrical shape. In addition, they assessed the drag force of real wood in a natural river.

Recently, several two-dimensional (2D) hydrodynamic flow models (Eulerian method) have been combined with driftwood transport models (Lagrangian method). Ruiz-Villanueva et al. (2014) developed Iber-wood model considering the force balances between water flow and driftwood, and they verified the model using a flume experiment. Persi et al. (2019) developed ORSA2D_WT. This model can reproduce the wood transport

by calculating multiple local forces from the four segments of the cylindrical wood body. Kang et al., (2019c) also carried out the simulations to reproduce both the wood transport and the bed changes using the model, which considers wood particles of the two-dimensionally connected spheres.

Such numerical ways are useful to easily demonstrate the wood motions and water flows, but these are required to a number of data for verifying the models in terms of the river scale (Ruiz-Villanueva et al., 2016a,b; Kang et al., 2019c). Thus, it would be appropriated to carry out either the experiments or the observations together with the numerical simulations.

The bed deformation with driftwood has been mainly conducted in the flume experiments (e.g., Welber et al., 2013; Bertoldi et al., 2014), and Kang et al. (2019) applied to the numerical simulation using those results. These researchers similarly presented the driftwood effect on bed morphology. In particular, their results indicated that bed morphology is dominant in the wood motions and the deposition patterns. However, those works dealt with the partially submerged braiding channel only. Thus, we should consider another channel geometry into the totally submerged alternating bar to understand more diverse morphodynamics considering the driftwood.

In this study, we carry out the flume experiments and numerical simulations to examine the effect of driftwood deposition patterns and bed deformation. To quantify the bed deformation based on potential hydrodynamic changes by driftwood, we estimate non-dimensional stream power index (NDSPI) and bed relief index (BRI). Then we compared the simulations with experimental results. This study shows useful data of interaction between the driftwood congestion and bed deformation. In addition, this work can suggest the treatments for driftwood and bar formations in the numerical and experimental ways.

2. METHODOLOGY

2.1 Experimental and computational setup

Figure 1 shows the flume domain (12 × 0.4 m^2) and computational domain (5 × 0.4 m^2). The computational domain is located within 3-8 m of the flume because this domain was gauged to obtain the bed elevation. The two experiments (hereafter, Exp1 and Exp2) were carried out to consider the two types of the time interval of wood supply: 5 s and 9 s, respectively. Herein, all flume experiments were conducted under the same hydraulic conditions as shown in Table 1. In the experiments, the time for generating the sand bar was 5 h under the initial flatbed with a constant slope (0.005 m/m). The flow discharge was 1.1 liter/s and we supplied wood pieces after the generation in the sand bars.

In the flume experiments, the initial angle of wood pieces was 90 degrees against the streamwise direction. Wood piece supply zone in flume experiments was set at the 1.5 m far from the target section to prevent the wave by wood supply (Kang et al. 2019a).

At the upstream of the computational domain (Figure 1), we set the diameter of the random generation for the wood piece as 0.1 m, and the initial angle of wood piece is random (0-360 degrees). In supplement of the wood pieces, we alternately input the 200 wood pieces including rootwads (100) and no rootwads (100) rootwad for Exp1 and Exp 2. The density of wood piece was 620 kg/m^3 and the diameter of wood piece was 0.01 m.

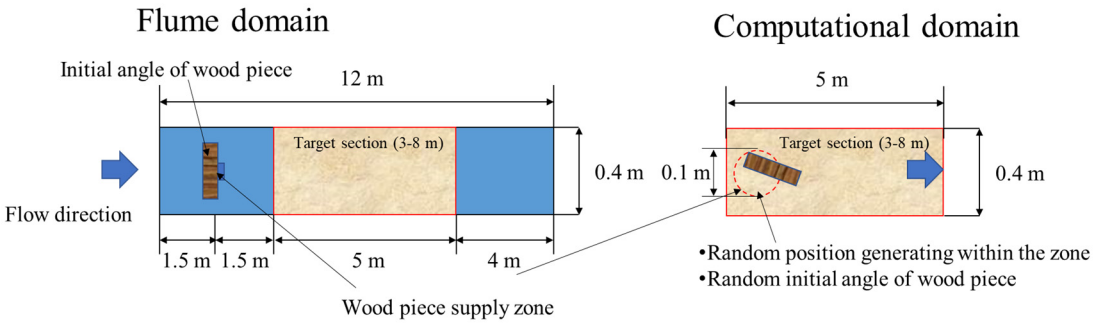

Figure 1. Flume (experiment) and computational domains

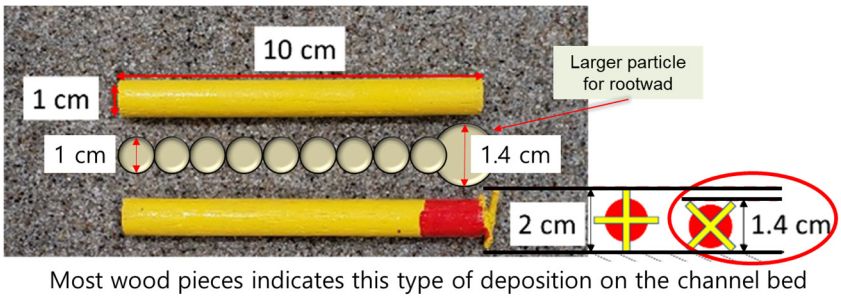

Figure 2. Profile of wood pieces and rootwad

The diameter of rootwad modeled as a "cross" shape was 0.02 m as shown in Figure 2. The deposition of this cross shape varied depending on the driftwood deposition (Figure 2). If the deposition happens with "+" angle, the diameter of the rootwad can be assumed to be 0.02 m. On the contrary, if the deposition happens with "×" angle, the diameter should be assumed to be 0.014 m. As most of wood pieces indicates this type of rootwad position on the channel bed, we thus considered "×" angle types in the simulations.

In the numerical simulation, we used the bed elevation of 9 s experiment only. The resolution of gauged bed elevation (Δx and Δy) was 0.001 × 0.02 m^2, and the uniform rectangular grid size of the computational domain was 0.02 × 0.02 m^2 to reduce the CPU time. To simulate the flows along with driftwood dynamics and bed morphology, we used a 2D plane solver, which is based on DEM and Nays2DH in iRIC software. In the water flow calculation, we employed the third-order total variation diminishing-monotonic upstream centered scheme for conservation laws (TVD-MUSCL) to solve the advection term of water flow and we considered the central scheme for the Reynolds stress term. A zero-equation-type turbulence model based on the shallow flow equations is also used.

The Manning roughness coefficient was 0.013 $s/m^{1/3}$, estimated by the Manning–Strickler formula using the averaged sediment diameter of 0.51 mm. To calculate the change of bedload flux by driftwood for each grid cell, the saturation ratio of an area of a deposited wood particle to the cell area is used. If the saturation ratio increases, the bedload flux increases, otherwise it decreases (Kang et al., 2019c). For the sediment transport, Ashida and Michiue's model (1972) was incorporated to estimate the bedload flux in the directions of streamwise and transversal, and a bank collapse model (Hasegawa, 1985) that considers the angle of repose (=30 [deg]) is combined in the Nays2DH.

For the model of driftwood dynamics (floating, sliding, and settling), we employed particle method based on DEM. In addition to floating on the water surface, this model considers both the change of draft for wood motion (CDM) and the bed friction force to consider the sliding and settling motion. To estimate the wood collision force, we assumed that the particles of wood piece are a soft sphere (Assumed Young modulus=100000 psi) and we employed Dash-pot-spring motion. Such method of the wood collision (based on DEM) has been widely known in this field (e.g., Gotoh et al., 2013; Kimura and Kitazono, 2019; Kang et al., 2019b), thus we omitted the description for the equations. The detail equations for hydrodynamic model and driftwood dynamics were described in the several works and iRIC website (Shimizu et al., 2014; Kang and Kimura, 2018; Kang et al., 2019b; Kang et al., 2019c; Kimura and Kitazono, 2019; International River Interface Cooperative (iRIC), 2020).

2.2 Refinement of wood collision model

In the present study, we found that the collision force by the dash-pot-spring model was reproduced well when wood pieces are floating on the water during the test of simulations. However, the collision force of the Dash-pot-spring model was exceedingly reduced by the bed frictions force of particle motion. Thus, the wood pieces in the simulations showed more depositions of wood pieces then our experiments. We, therefore, conceptually refined the wood collision process.

Table 1. Model parameters

Parameter	Value
Flow discharge	1.1 liter/s
Computational domain size (uniform rectangular grid shape)	5 m × 0.4 m
Bed slope	0.005 m/m
The resolution of gauged bed elevation (Δx and Δy)	0.001 m × 0.02 m
The resolution of computational grid length (Δx and Δy)	0.02 m × 0.02 m
Manning roughness coefficient	0.013 $sm^{-1/3}$
Uniform grain size	0.51 m/m
The total input number of driftwood pieces per case	200 (=100 rootwad + 100 no roowad)
Critical draft for wood motion (trunk particle)	0.0057 m
Critical draft for wood motion (root wad particle)	0.008 m
Static bed friction coefficient	0.5
Kinematic bed friction coefficient	0.2
Rolling bed friction coefficient	0.075
Eddy viscosity for zero equation	0.4
Time for experiment and simulation	40 min
Time interval for wood supply	5 s or 9 s
Range of initial angle of wood piece	0-360 [degrees]
Diameter of wood pieces generating zone	0.1 m
Poisson ratio	0.3
Young modulus	100000 psi
Time step of driftwood motion in simulation	0.00001 s
Time step of water flow and bed deformation in simulation	0.01 s

Table 2. Experimental and simulation cases

	Time interval of wood supply	Random parameter
Exp1	5 s	Absent
Exp2	9 s	Absent
Sim1	5 s	· Generating position of wood pieces within the supply zone · Initial angle of wood piece
Sim2	5 s	
Sim3	5 s	
Sim4	9 s	
Sim5	9 s	
Sim6	9 s	

We considered two types of wood collisions: 1) dashpot-spring motion velocity when driftwood is floating; 2) water flow velocity when the state of driftwood is sliding or deposition.

The activation of water flow velocity in the wood collision was restricted within the lower water depth region than CDM. Otherwise, the collision velocity is determined by the dash-pot-spring motion when a wood piece is floating on out of the lower water depth. This wood collision system in the numerical model is expressed as follows:

$$\begin{cases} \mathbf{u}_p = \mathbf{u}_p + \Delta t\mathbf{F}, & \text{if } h > \text{CDM} \\ \mathbf{u}_p = \mathbf{u}_w, & \text{if } h \le \text{CDM} \end{cases} \quad (1)$$

where $\mathbf{u}_p$ is the component of particle velocity vector; $\mathbf{u}_w$ is water flow velocity vector; Δt is time step, $\mathbf{F}$ is collision force between wood particles; h is water depth; CDM is critical draft for wood motion. Note that Equation 1 only considers the collision forces, except for other forces such as drag force.

This conceptual method can reproduce well the time changes in the number of stored wood pieces. Such results are explained in the section of "3. RESULTS AND DISCUSSION"

To compare the wood supply effect depending on the time interval, we separately conducted the experiments with Exp1 and Exp2. In the simulations, we conducted three times simulations for each case (5 s and 9 s). Sim1-3 are 5 s cases, and Sim4-6 are 9 s cases for time interval for wood supply.

2.3 Hydrodynamical bed morphology evaluation

NDSPI indicates the potential change of sediment transport on the channel bed. If NDSPI increases, the sediment transport becomes active. In addition, if NDSPI significantly changes, it implies that the bar formation systems may be altered into other bar formation processes (e.g., alternating bar, braiding channel, and channel meander). The equation of NDSPI was proposed by Hoey (1992) as follows:

$$\omega^* = \bar{q}\bar{S}\,[(S_s - 1)g{d_m}^3]^{-0.5},\ q = \bar{V} \times \bar{d} \quad (2)$$

where, ω^* = NDSPI, $\bar{q}$ = unit water discharge (m^2s^{-1}), $\bar{V}$ = cross sectional averaged velocity (ms^{-1}), $\bar{\bar{d}}$ = cross sectional averaged water depth (m), $\bar{S}$ = cross sectional averaged local channel slope between target grid point and neighboring downstream grid point, S_s = submerged specific gravity of sediment (≈1.65), g = acceleration due to gravity ($9.81ms^{-2}$), and d_m = mean grain size (m).

In addition to the stream power, we estimated the time changes in bed configurations using bed relief index (Hoey and Sutherland, 1992; Kang et al., 2018) to evaluate the magnitude of the channel variation. When bed relief index becomes 0, the channel bed becomes totally flatbed with constant slope.

3. RESULTS AND DISCUSSION

3.1 Results of the simulations and the experiments

Figure 3 shows the simulation results for the wood (with/without rootwad) deposition patterns, and the channel variation profile (along the bed slope) together with the experimental results. Note that the experimental results approximately show the driftwood deposition patterns without an exact scale.

The reproduced wood pieces are significantly different from the experimental results. This is because the inlet boundary condition causes to easily move the driftwood in the upstream region. Thus, most driftwood are deposited in the downstream region.

In the experimental results, the final number of stored wood pieces in 5 s (Exp1) and 9 s (Exp2) are 24 and 45, respectively. The case of simulations (Sim1-6) are 33, 32, 26, 44, 49, 47, respectively.

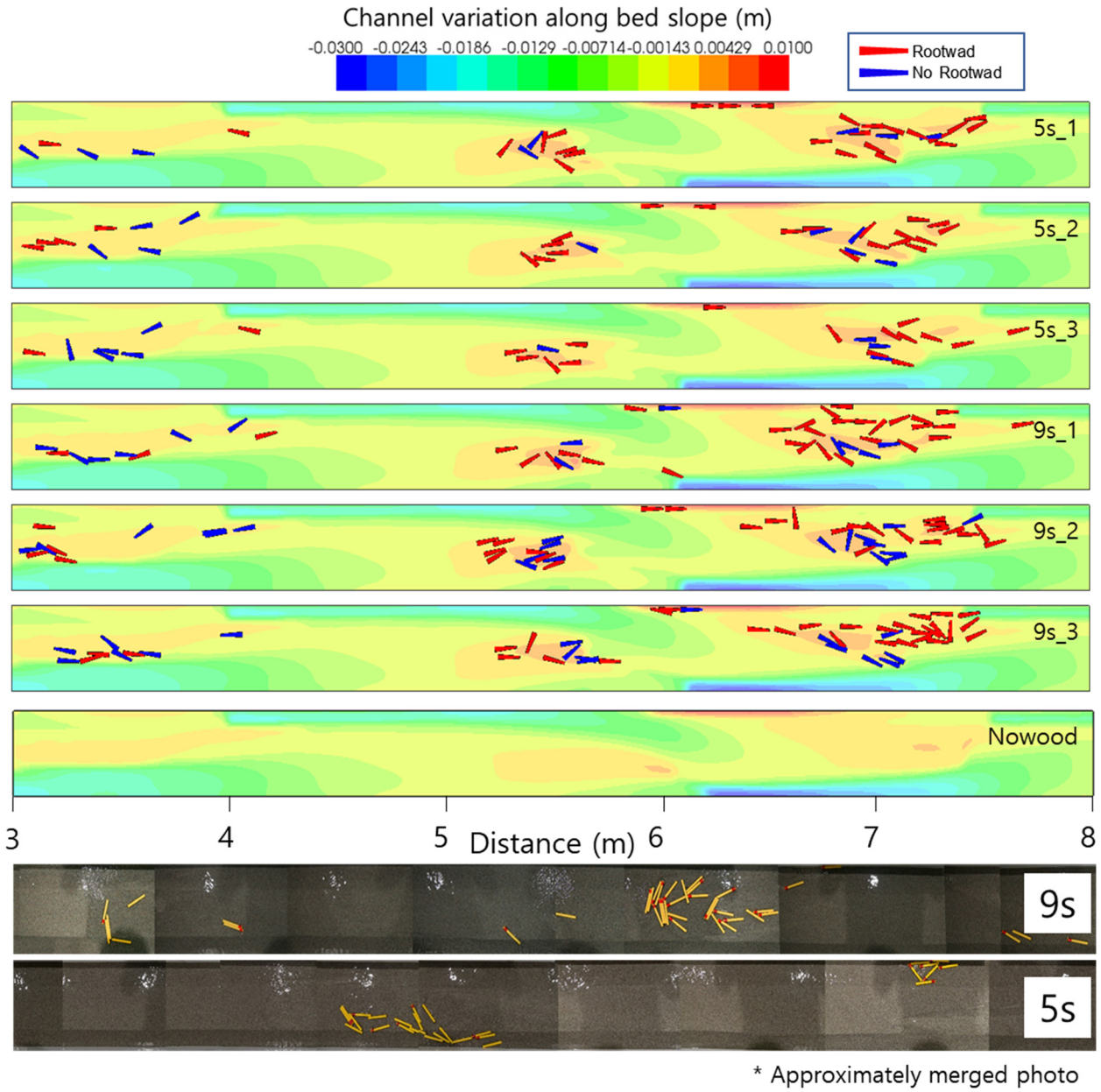

Figure 3. Driftwood deposition patterns in the simulations and experiments.

Since we used only 9 s bed elevation in the simulations of 5 s and 9 s, the simulation results of 5 s could not be specifically compared with the experimental result of 5 s. In future work, we, therefore, would obtain the bed elevation data of 5 s and compare with the simulation results of 5 s based on the obtained bed profile.

In the simulations and the experiments, the wood jams are deposited on the bar crest because water depth is lower than CDM. Those wood jams disturb the motion path of other wood pieces, which is coming from upstream. In additions, they also capture the moving wood pieces, so that those wood pieces are formed into wood jams, again. Water flow velocity near the wood jams increases and causes bed erosion. On the contrary, channel bed increases within the location of wood jams. This is because the water flow velocity decreases and the sediment deposition becomes active in the location of the wood jam.

Figure 4 shows the channel variation along the constant bed slope before/after the wood supply to clearly show the driftwood deposition patterns. We observed the small size erosions as shown in Figure 4 (the bed elevation is 9 s case only). However, this kind of erosion is not reproduced in the simulations, because the grid size is larger than the wood diameter, so that such smaller erosions could be neglected in the simulation. Thus, it should be refined to more advance the driftwood model. The sub grid model would be one of alternative methods to reproduce the smaller erosion.

3.2 Bed deformation and time changes in the number of the stored wood pieces

Figure 5 shows the time changes in the number of stored wood pieces. Herein, “Ave_logs_5s” and “Ave_logs_9s” indicate the averaged number of wood pieces in each case (5 s and 9 s), respectively. The time interval of wood

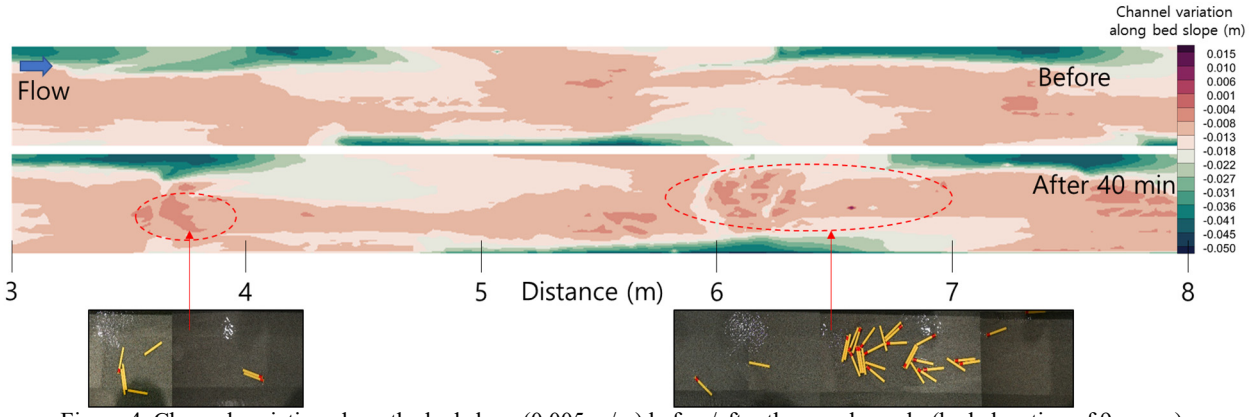

Figure 4. Channel variation along the bed slope (0.005 m/m) before/after the wood supply (bed elevation of 9 s case)

supply can affect to control the number of stored wood pieces as shown in this figure. In other words, the time interval of wood supply activates the wood collisions by the generated floating wood pieces.

The simulated number of wood pieces are overestimated than the experimental results as shown in Figure 5. This is because the model cannot reproduce the local sediment transport around the driftwood. In particular, the scour erosion on the contact bed between the channel bed and driftwood is significantly underestimated. It causes to disturb the degradation of the channel bed and to retain the lower submerged water depth than CDM. As a result, underestimated erosion allows the stable deposition to the wood pieces.

Bar migration patterns are changed by the wood jam as shown in Figure 4. The speed of bar migration shows an unclear pattern in the whole domain, but wood jams cause the local erosion near the deposited location. Consequently, the effect of wood jams is not dominant to the whole domain, but wood jams can locally affect the bed deformation. The channel geometry rather influences on the jam formation and single driftwood deposition (Kang et al., 2019c).

3.3 Hydrodynamical bed morphology evaluation in the simulations considering driftwood

Figures 6 and 7 show time changes in NDSPI and BRI, respectively. To clearly indicate the driftwood effect, we simulated an additional case without driftwood. In those Figures, “nowood” means the simulation without driftwood.

The NDSPI decreases during 0-900 s. This is because the channel slope near the upstream region significantly changes by the transversal distribution of flow velocity. Herein, the flow velocity at the upstream boundary is iteratively calculated using the channel variations and the dummy discharge of upstream cross-section, to obtain the same boundary flow discharge with observed flow discharge. After the 900 s, the bar migrations actively initiated in the whole of domain, thus NDSPI increases.

The simulations with driftwood show larger BRI, comparing with nowood case. On the contrary, nowood case shows larger values of NDSPI and smaller values of BRI. As shown in Figure 4, such changes of NDSPI and BRI are caused by the local deformation of channel bed due to the driftwood effect.

3.4 Limitation of refined model for wood collision on the moveable channel bed

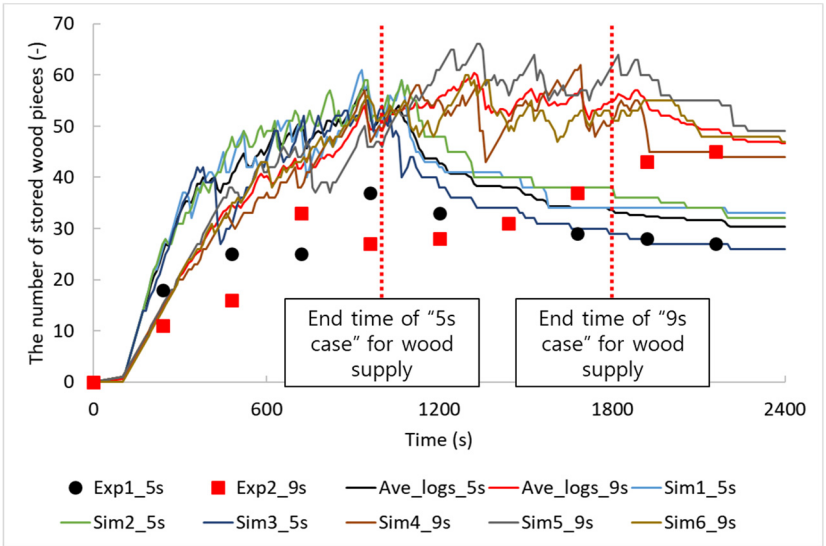

Figure 5. Time changes in the number of wood pieces

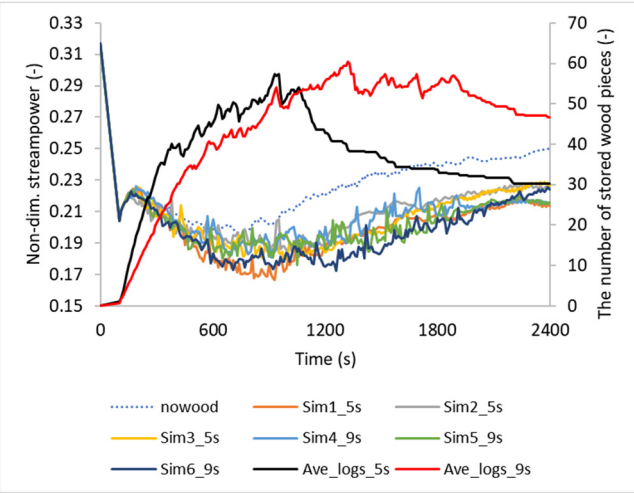

Figure 6. Time changes in non-dimensional stream power

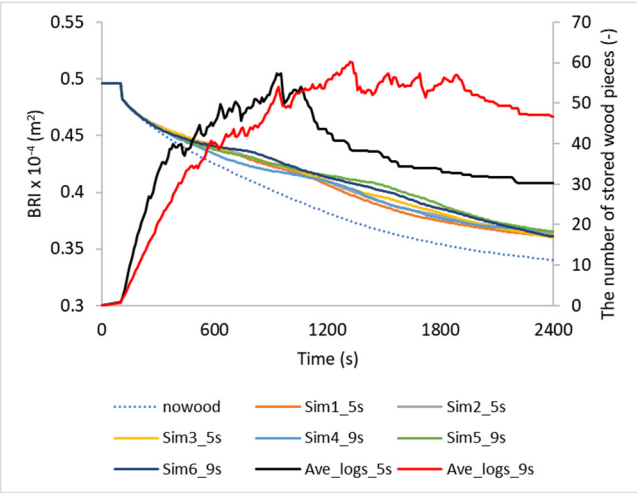

Figure 7. Time changes in bed relief index

To refine the wood collision model, we employed the conceptual wood collision model together with the dashpot-spring model, and we obtained acceptable results about the number of stored wood pieces. However, the refined model is insufficient to explain the mechanism of physical collisions. In addition, this model may be inappropriate to reproduce the driftwood deposition patterns under the different computational conditions (hydraulic conditions, and fixed bed). Hence, the refined model should be advanced in terms of physical phenomena. For instance, the present model neglected the seepage flow on the contact area between driftwood and channel bed. On the contrary, in the experiments, we observed the active seepage flow, and it caused to remobilize the deposited driftwood together with the sediment transport. Such phenomena accordingly can be an important refinement point for numerical reproducibility.

4. CONCLUSIONS

In the experiments (Exp1 and 2), the time interval of wood supply may affect the final number of stored wood pieces. This is because the greater number of wood pieces allows more active collisions with floating motion. The simulations (Sim1-6) also partially reproduced the number of stored wood pieces.

Along with the experimental results, NDSPI and BRI showed that the driftwood can influence bar formation through the local deformations on the channel bed.

Our results can be useful data to take account of the relationship between bed deformation and driftwood. In particular, this study enhanced the understanding of the totally submerged channel bed, so it can be one of the important cases for driftwood study. For more detailed discussions, such as the refinement of the wood collision model, we would additionally compare the experimental results with numerical model refinement in the future works.

ACKNOWLEDGMENTS

We are thankful to Japan Society for the Promotion of Science (JSPS) for providing funding for this research (18F18359).

REFERENCES

Ashida, K. and Michiue, M. (1972). Study on hydraulic friction and bedload transport rate in alluvial streams. *Trans. JSCE*, 206: 59–69.

Bertoldi, W., Welber, M., Mao, L., Zanella, S. and Comiti, F. (2014). A flume experiment on wood storage and remobilization in braided river systems. *Earth Surf. Processes Landforms*, 39: 804-813.

Braudrick, C.A., Grant, G.E. (2001). Transport and deposition of large woody debris in streams: a flume experiment. *Geomorphology*, 41: 263–283.

Braudrick, C.A., Grant, G.E., Ishikawa, Y. and Ikeda, H. (1997). Dynamics of wood transport in streams: a flume experiment. *Earth Surface Processes and Landforms*, 22: 669–683.

Davidson, S.L., MacKenzie, L.G. and Eaton, B.C. (2015). Large wood transport and jam formation in a series of flume experiments. *Water Resour. Res.*, 51: 10065–10077, doi:10.1002/2015WR017446.

Gippel, C.J., O´Neil, I.C. and Finlayson, B.L. (1992). The hydraulic basis of snag management. Centre for Environmental Applied Hydrology, Department of Civil and Agricultural Engineering, University of Melbourne, Australia.

Gotoh, H., Okayasu, A. and Watanabe, Y. (2013). Computational wave dynamics. Advanced series on ocean engineering, World Scientific, Singapore, 87.

Hasegawa, K. (1985). Hydraulic study on alluvial meandering channel planes and bedform topography-affected flows. Ph.D. dissertation, Hokkaido University, Sapporo, Japan.
Hoey, T. and Sutherland, A. (1991). Channel morphology and bedload pulses in braided rivers: A laboratory study. *Earth surf. Process. Landforms*, 16: 447-462.
Hoey, T. (1992). Temporal variations in bedload transport rates and sediment storage in gravel-bed rivers. *Physical Geography*, 16(3): 319-338.
International River Interface Cooperative (iRIC). (2020). Available Online: http://i-ric.org/en.
Kang, T., Kimura, I. and Shimizu, Y. (2018). Responses of bed morphology to vegetation growth and flood discharge at a sharp river bend. *Water*, 10(2): 223, 2018, DOI: 10.3390/w10020223.
Kang, T. and Kimura, I. (2018). Computational modeling for large wood dynamics with root wad and anisotropic bed friction in shallow flows. *Advances in Water Resources*, 121: 419-431.
Kang, T., Kimura, I. and Onda, S. (2019a). Bed morphology responses with driftwood deposition patterns on an alternating bar through a flume experiment and a computation, *Journal of Japan Society of Civil Engineers*, Ser., B1 (Hydraulic Engineering), 75(2): I_319-324**.**
Kang, T., Kimura, I. and Onda, S. (2019b). Computational modeling for driftwood collision dynamics in shallow flows considering projection area, root wad and anisotropic bed friction. *Proceeding of IAHR-World congress 2019*, Panama City, Panama.
Kang, T., Kimura, I. and Shimizu, Y. (2019c). Numerical simulation of large wood deposition patterns and responses of bed morphology in a braided river using large wood dynamics model. *Earth Surf. Processes Landforms*, doi: 10.1002/esp.4789.
Kimura, I. and Kitazono, K. (2019). Effects of the driftwood Richardson number and applicability of a 3D–2D model to heavy wood jamming around obstacles. *Environmental Fluid Mechanics*, doi.org/10.1007/s10652-019-09709-6.
Persi, E., Petaccia, G., Sibilla, S., Brufau, P. and García-Navarro, P. (2019). Calibration of a dynamic Eulerian-lagrangian model for the computation of wood cylinders transport in shallow water flow. *Journal of Hydroinformatics*, 21(1): 164-179.
Persi, E., Petaccia, G., Fenocchi, A., Manenti, S., Ghilardi, P., and Sibilla, S. (2019). Hydrodynamic coefficients of yawed cylinders in open-channel flow. *Flow Measurement and Instrumentation*, 65: 288‑296.
Ruiz-Villanueva, V., Bladé, E. and Sánchez-Juny, M. (2014). Two-dimensional numerical modeling of wood transport. *Journal of Hydroinformatics*,16(5): 1077-1096.
Ruiz-Villanueva, V., Wyżga, B., Zawiejska, J., Hajdukiewicz, M. and Stoffel, M. (2016a). Factors controlling large-wood transport in a mountain river. *Geomorphology*, 272: 21–31.
Ruiz-Villanueva, V., Wyzga, B., Hajdukiewicz, H., Stoffel, M., Wyżga, B., Hajdukiewicz, H., Stoffel, M., Wyzga, B., Hajdukiewicz, H. and Stoffel, M., (2016b). Exploring large wood retention and deposition in contrasting river morphologies linking numerical modelling and field observations. *Earth Surf. Processes Landforms*, 41: 446–459.
Shields, F.D. and Alonso, C.V. (2012). Assessment of flow forces on large wood in rivers. *Water Resour. Res.*, 48. W04516, doi:10.1029/2011WR011547.
Shimizu, Y., Takebayashi, H., Inoue, T., Hamaki, M., Iwasaki, T. and Nabi, M. (2014). Nays2DH solver manual. Available Online: http://i-ric.org/en.
Welber, M., Bertoldi, W. and Tubino, M. (2013). Wood dispersal in braided streams: Results from physical modeling. *Water Resour. Res*., 49: 7388–7400, doi:10.1002/2013WR014046.